RSC Advances

This is an *Accepted Manuscript*, which has been through the Royal Society of Chemistry peer review process and has been accepted for publication.

Accepted Manuscripts are published online shortly after acceptance, before technical editing, formatting and proof reading. Using this free service, authors can make their results available to the community, in citable form, before we publish the edited article. This *Accepted Manuscript* will be replaced by the edited, formatted and paginated article as soon as this is available.

You can find more information about *Accepted Manuscripts* in the Information for Authors.

Please note that technical editing may introduce minor changes to the text and/or graphics, which may alter content. The journal's standard Terms & Conditions and the Ethical guidelines still apply. In no event shall the Royal Society of Chemistry be held responsible for any errors or omissions in this *Accepted Manuscript* or any consequences arising from the use of any information it contains.

ROYAL SOCIETY OF CHEMISTRY

www.rsc.org/advances

Please do not adjust margins

Journal Name

ARTICLE

Synthesis, Characterization and Fabrication of Ultrathin Iron Pyrite (FeS_2) Thin Films and Field-effect Transistors

Received 00th January 20xx,
Accepted 00th January 20xx

DOI: 10.1039/x0xx00000x

www.rsc.org/

Xi Liu[a,b,c], Zhaojun Liu[*a,b,c] Jacob Y. L. Ho[c], Man Wong[c], and Hoi Sing Kwok[c]

We reported a synthesis of an ultrathin FeS_2 thin film via thermal sulfurization of an iron thin film and its fabrication process for field-effect transistors. Reaction time was found to be essential for the growth of the crystallized FeS_2 thin film. The thickness of Fe increased from 10nm to 35nm after the reaction. The FeS_2 thin film has a resistivity of 0.345 Ω·cm and a Hall mobility of 7.1 cm^2 V^{-1} s^{-1}, with a carrier concentration of 2.89×10^{18} cm^{-3} The fabricated FeS_2 transisotrs have a reported highest current on/off ratio of 3.94×$10^4$and Ion of 0.117 mA. Moreover, the FeS_2 based transistor not only broader the applications of pyrite, but also provides a platform for investigtion of FeS_2 materials. Temperature-dependent electrical transport measurements confirmed the rich intrinsic defect states in the FeS_2 thin film, which indicates that reducing intrinsic defect might be the key issue to further improve the device performance.

Introduction

Iron pyrite (FeS_2), which is also known as fool's gold, is an intriguing semiconductor that is an abundant mineral in the Earth.[1] It is widely found in quartz veins, sedimentary rocks and coal beds, and it has attracted continuous interest since the 1970s because it is a rich resource and has unique properties.[2–5] FeS_2 has a small band gap (0.8-0.95 eV) and a large light absorption coefficient ($\alpha = 6 \times 10^5\ cm^{-1}, \mathrm{h\nu} > 1.3\ \mathrm{eV}$), making it a promising candidate for solar energy conversion.[6,7] The highest reported electron carrier mobility is approximately 360 $cm^2 V^{-1} s^{-1}$, with a minority carrier diffusion length of 0.1-1 μm.[8] These properties make FeS_2 a potential alternative thin layer absorber for photovoltaic (PV)[9] and photo-electrochemical solar cells.[10]

However, despite all the excellent properties of pyrite, the best pyrite-based solar cell only has an energy conversion efficiency of 3%.[11] Researchers have experienced difficulties in improving its performance, primarily because of the low fill factor (approximately 0.5) and open circuit voltage (≤ 200 mV) caused by the high recombination loss and the rich density of the sulfur defect states.[12,13] Additionally, the doping mechanism and method of FeS_2 materials is not clear.. These disadvantages prevent FeS_2 from creating a p-n homojunction or a p-i-n junction in solar cells.[14] With the emergence of other promising materials for thin film solar cells, including $CuInGaSe_2$,[15,16] the potential of FeS_2 as a candidate for solar PV applications has waned.

Recently, FeS_2 has attracted interest once again because of its low cost and potential applications for field-effect transistors (FETs).[17] Several new synthesis methods have been described to improve the FeS_2 thin film quality and properties, such as chemical vapor deposition (CVD),[18,19] the sulfidation of Fe_2O_3,[20] molecular beam epitaxy (MBE),[21] sputtering,[3,22] sol-gel,[23] and electrodeposition.[24] Moreover, substantial effort has been focused on the low-cost colloidal synthesis of pyrite nanocrystals.[10,13] Different pyrite morphologies, such as nanowires, nanobelts and nanoplates,[9] have also been synthesized and reported.

These synthetic improvements have led to broader applications besides PV and Photo-electrochemical solar cell. For instance, Qihua Xiong et al.[25] used FeS_2 thin film as counter electrodes for Dye-Sensitized Solar Cells (DSSC) utilizing I^{3-} /I^- and Co(III)/Co(II) as the electrolyte. The new (DSSC) gives a photoconversion efficiency around 8% which is comparable to Pt. Song Jin et al.[26] utilized FeS_2 nanowires as cathodes materials in Li-ion battery using a liquid electrolyte, which retains a discharge energy density of 534 Wh kg^{-1} at 0.1C rate while has a discharge capacity of 350mAh g^{-1}. Other potential usage including hole transportation[9], photodetector[27], and even in agriculture[28]. FeS_2 is earth abundant and low cost materials. Hence the development in FeS_2 application will benefit many different fields and further lower the cost for industry.

However, although FeS_2 has a very unique electrical properties, its potential usage in FETs has not yet been fully developed. Figure 1 shows the computational band structure of FeS_2

[a.] Sun Yat-sen University–Carnegie Mellon University Joint Institute of Engineering, Sun Yat-sen University, Guangzhou, China. E-mail: eezhj@ust.hk
[b.] Sun Yat-sen University–Carnegie Mellon University Shunde International Joint Research Institute, Sun Yat-sen University, Guangdong, China
[c.] State Key Lab on Advanced Displays and Optoelectronics, Department of Electronic and Computer Engineering, Hong Kong University of Science and Technology, Clear Water Bay, Kowloon, Hong Kong
[d.] † The FeS_2 FET device parameter calculations and Structure characterization and optical properties of FeS_2 thin film on quartz substrate are provided in the Supporting Information. This material is available free of charge via the Internet at **http://pubs.acs.org.**

Please do not adjust margins

RSC Advances Accepted Manuscript

compared with those of other transition-metal dichalcogenides (TMDs) and commonly used semiconductors.[29] The band gap of FeS_2 is slightly smaller than that of silicon (1.1 eV), which makes it a natural alternative material for electrical devices. Other TMD materials, including MoS_2 (~1.29 eV) and WS_2 (~1.4 eV), usually have larger band gaps. Although there have been a few research reports addressing FeS_2 FET devices, the performance of these devices remains far from satisfactory. For example, although a recently reported FeS_2 nanowire FET device has a mobility of approximately 0.1-0.2 $cm^2\ V^{-1}\ s^{-1}$ at a carrier concentration of approximately $2.9\times10^{18}\ cm^{-3}$, it is difficult to pinch off, which leads to a low I_{on}/I_{off} ratio for the output current.[30,31] Some of the reported FeS_2 thin film materials electrical properties is listed in Table 1 and compared with our work. A further understanding of the electrical transportation for materials and device is needed to further improve the performance of FeS_2.

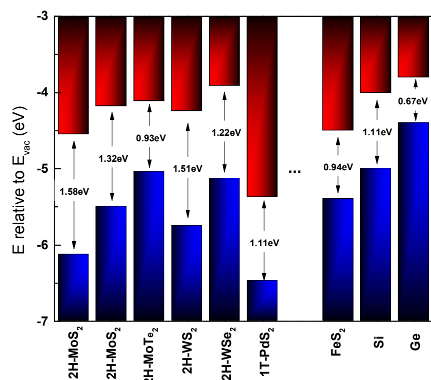

Figure 1. Absolute band edge positions of the selected materials

Table 1. Reported FeS2 materials electrical properties

Mobility ($cm^2\ V^{-1}\ s^{-1}$)	Carrier Concentration (cm^{-3})	Thickness (nm)	Resistivity (Ω·cm)	Reference
1.450	7.69×10^{18}	90±10	0.5605	23
0.271	2.1×10^{20}	70	0.11	32
11.8	2.5×10^{18}	400	0.58	33
2.12	4.90×10^{18}	200±50	0.58	25
7.1	**2.89×10^{18}**	**35**	**0.345**	**This work**

In order to develop the application for FeS_2 based FET, we studied the growth of FeS_2 and improve the quality of the FeS_2 thin film. We investigated the simplest synthesis among with the methods mentioned above: ex-situ thermal sulfidation of an Fe thin film as Figure 2.We synthesized a very thin films under atmosphere while many other similar methods require vacuum system. We also manage to obtain an ultrathin FeS_2 film with low carrier concentration. The best FeS_2 synthesized using this sulfidation time has a mobility of 7.1 $cm^2\ V^{-1}\ s^{-1}$ and a Hall carrier concentration of approximately $2.9\times10^{18}\ cm^{-3}$.It is a general method for synthesizing FeS_2 thin film on different substrate, like quartz, for various application. For various applications, we can implement our method on selected substrates, like quartz, Al_2O_3, ZrO_3 etc. We also developed a procedure for the fabrication of FeS_2 thin film FETs. We studied the device electrical properties giving a I_{on} at 0.117mA with an I_{on}/I_{off} ratio of 3.94×10^4, which is much higher than previously reported FeS_2 transistors. The FeS_2 based FETs provides us a general platform to study the properties of FeS_2. For instance, we investigated the temperature dependence electrical measurement and it revealed a Mott variable range hopping (VRH) electron transport mechanism of FeS_2 at low temperatures. It suggests that the carrier transport is dominated by intrinsic defects, which is consistent with previous reports.[34] It indicates improve the performance of FeS_2 needs to focus on how to reduce the defects states. Further research on FeS_2 devices can also draw information from related works, such as the research on MoS_2 FETs, which demonstrated that high-k dielectric gate materials might further increase the device performance and modulation capablity.[35]

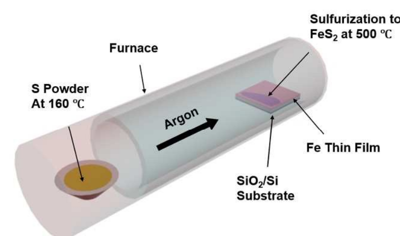

Figure 2. Schematic diagram of the home-built CVD reaction system

Experiment Section

FeS_2 Thin Film Fabrication

The FeS_2 thin film was synthesized via two commonly used two-step ex-sulfurization processes. First, we deposited 10 nm of an Fe thin film on a pre-prepared SiO_2/Si substrate using D.C. magnetron sputtering with an iron target. The SiO_2 layer was approximately 300 nm and was deposited by low pressure chemical vapor deposition (LPCVD). The film was then placed in a custom-designed chemical vapor deposition furnace system on a quartz boat. The furnace set up is shown in Figure 2, the sulfur was placed upstream, and the film was placed downstream. The sulfur was heated by a silicone rubber heat belt and controlled by a digital temperature controller. At 160 °C, the sulfur existed in both the liquid and gas phases. The mixture was sent into the furnace with argon at a rate of 200 sccm. The sulfurization temperature was held constant at 500 °C with a ramping speed of 10 °C per min, as reported by other studies.[6,9,14] We used reaction times of 180, 240 and 360 min, and the sulfur flow was stopped immediately after the

RSC Advances Accepted Manuscript

This journal is © The Royal Society of Chemistry 20xx

reaction by removing the heat belt. After the sulfurization process, the system cooled to room temperature at the natural cooling rate. The same method is also used on quartz substrate with reaction time for 240 min for optical properties characterization.

FeS_2 FET Fabrication

The as-synthesized FeS_2 thin film was first cleaned using four cycles of deionized (DI) water and then dry-etched with an induced coupled plasma (ICP) etcher after a photolithography process. After dry etching, the drain and source electrodes were defined by a second photolithography process, and then, Ni (200 Å)/Ti (700 Å)/Au (300 Å) stack layers were deposited via e-beam evaporation as the source/drain metal. Acetone and isopropanol were used for the lift-off process, and the device was cleaned with DI water.

Characterization

The thin film X-ray diffraction (TFXRD) pattern of the as-synthesized sample was collected on an Empyrean (PAN analytical) Diffractometer using Cu Kα radiation. The tube current and tube tension were 40 mA and 40 kV, respectively. The data were collected from 20 degrees to 60 degrees with a measurement time of 1 second and 0.06 degrees per step. Raman spectra of the as-synthesized sample were collected on an InVia (Renishaw) confocal microscope using an Ar ion laser (514.5 nm and 50 mW).The resistivity, Hall mobility and carrier concentration were collected using a Resistivity/Hall Measurement System, Model HL5500PC (Bio-Rad). Silver paste was placed onto the thin film, which was then used for the four point measurement. The Atomic Force Microscopy (AFM) image was acquired using a Nanoscope-Multi Mode/Dimension 3100 system. The X-ray photoelectron spectroscopy analysis was performed with a PHI 5600 (Physical Electronics) surface analysis system with a monochromatic Al Kα X-ray source (1486.6 eV). Temperature dependence measurement was conducted using the Physical Property Measurement System (Quantum Design). Electrical measurements were collected with a Keithley 2182A nanovoltmeter and a 6221 ac/dc source.

Results and Discussion

X-ray diffraction is the primary technique to determine the phase and quality of a thin film. Because of the small thickness, thin film X-ray diffraction (TFXRD) was used in our experiments. The XRD pattern of the as-synthesized FeS_2 thin film is plotted in Figure 3, including the 180-, 240- and 360-min samples. All the peaks can be indexed to pyrite (JCPDS no. 00-026-0801), marcasite (JCPDS no.00-003-0795) and silicon (JCPDS no. 00-003-0544). Increasing the sulfurization time clearly results in an orientation preference and a phase change in the FeS_2 thin film. The 180-min and 240-min samples do not show the obvious existence of a marcasite phase, whereas the 360-min sample has clean peaks that represent a marcasite phase. It has been reported that the lattice constant of FeS_2 ranges from 5.428 to 5.407 Å because of the sulfur vacancies.[36,37] In our experiment, the average lattice parameter is 5.418 Å, which agrees with previous reports.[9]

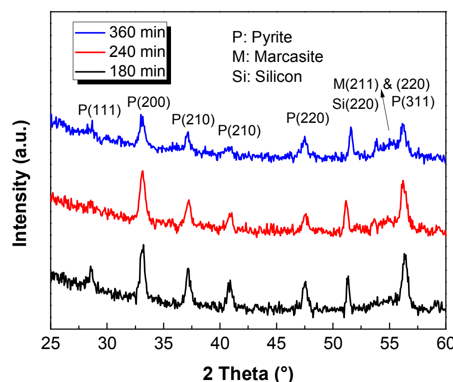

Figure 3. XRD patterns of the 180-, 240- and 360-min FeS_2 thin film

To further investigate the FeS_2 phase, confocal micro-Raman spectroscopy was used. It has been shown that Raman spectroscopy is more sensitive to different phases of FeS_2, and it is widely used in characterization. The Raman spectrum in Figure 4 for the 180-min sample shows three peaks at 338 (S_2 libration, E_g), 372 (S–S in-phase stretch, A_g) and 424 cm^{-1} (coupled libration and stretch, $T_{g(3)}$) that belong to pyrite.[10,13,38] Increasing the sulfurization time to 240 min causes a blue shift of the peaks from 338 to 339 cm^{-1},from 372 to 374 cm^{-1} and 424 to 427 cm^{-1}. The peak further blue shift to 341,376 and 427 cm^{-1} respectively when the reaction time increase to 360 min. It also generated of a marcasite peak at approximately 320 cm^{-1}, which agrees with the TFXRD result. We attribute the blue shift to a strong interaction between the S-S and Fe-S bonds because of the longer annealing time.[9,39,40]

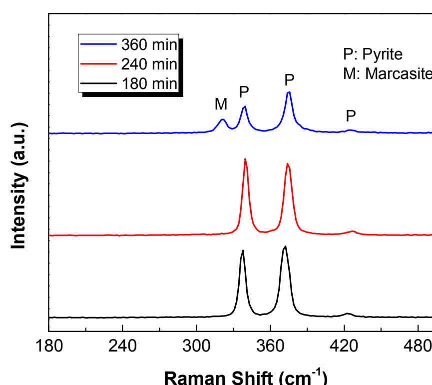

Figure 4. Raman spectra of the 180-, 240- and 360-min FeS2 thin film

AFM is a useful technique to study the morphology of thin films. In Figure 5, the reaction time can be seen to have a critical impact on the thin film surface. For the reaction time of

RSC Advances Accepted Manuscript

180 min shown in Figure 5a, the sample surface is extremely uneven with a surface roughness of approximately 17.47 nm. This sample is likely in the process of crystallization, and hence, the quality of the sample is poor. The gain is difficult to distinct. For the reaction time of 240 min shown in Figure 5b, the quality of the thin film is clearly improved. The small grains are evenly distributed on the substrate, and the grain size is approximately 80 nm, which is comparable to reported results for other sulfurization methods.[25] The surface roughness is also reduced to 6.41 nm. However, when the reaction time is increased to 360 min, the quality of the thin film becomes worse. The grains start to grow together and create small discontinuous areas, as shown in Figure 5c, which gives a grain size around 90nm. The surface roughness of the 360-min sample is slightly larger than for the 240-min sample (approximately 7.7 nm). The grain size is average of 50 gains in the AFM image.

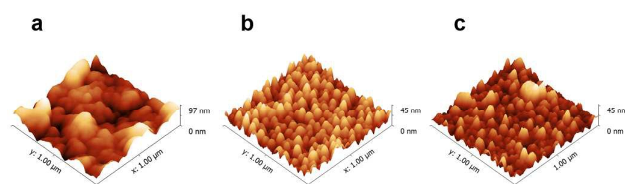

Figure 5. AFM images of different samples

XPS was then used to determine the elemental composition of the FeS_2 thin film surface. The XPS spectra of the 240-min sample are shown in Figure 6a. The peak at a binding energy of 162.4 eV is attributed to intrinsic bulk-like disulfides (BD) and belongs to S $2p_{3/2}$. S $2p_{1/2}$ has a peak at 163.5 eV, which is also characteristic of FeS_2.[13,41] Additionally, a small shoulder at 161.3 eV is attributed to surface disulfides (NSD and SD) on the {100} surface of iron pyrite caused by sulfur vacancies.[12,13] The peak at 164.8 eV is often described as high energy, and it is caused by a core hole effect, as discussed in recent papers.[13,42] All the results show that the FeS_2 thin film surface contains many sulfur defects, which will be discussed later in the paper. Figure 6b reveals the binding energies of the Fe 2p. The peaks at 707.1 eV and 719.8 eV belong to Fe-S $2p_{3/2}$ and Fe $2p_1/2$, respectively.[20] The small peak at approximately 711 eV is attributed to Fe-O and is the result of exposure to air.[43]

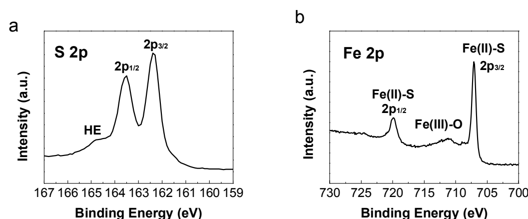

Figure 6. XPS spectra of the 240-min FeS_2 sample

The optical property of the FeS_2 thin film of our synthesis is also investigated. We grew FeS_2 thin film on quartz substrate. Raman spectrum showed the FeS_2 has very good quality in Figure S1. Detail of the optical property can be seen in Figure S2.

The electrical properties of the FeS_2 thin film were studied and are shown in Figure 7. The 240-min sample shows superior properties compared with the 180- and 360-min samples, primarily because of the improved crystallization, its mobility and carrier concentration are suitable for FETs. The values recorded for these properties are about 2.9×10^{18} cm^{-3} and 7.13 cm^2 V^{-1} s^{-1}, respectively, which are relatively high compared with other reports.[10,34,44] Although the 360-min sample shows some discontinuity, it maintains a high conductivity because of the larger grain size.

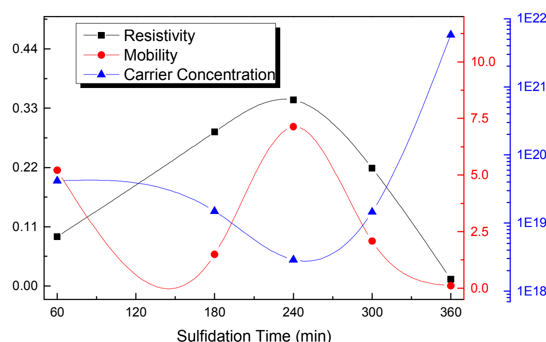

Figure 7. Electrical properties of different samples of FeS_2.

Based on the electrical properties of the FeS_2 thin film, we fabricated FeS_2 FETs using the 240 min sample, as mentioned in the experimental section. A schematic and an optical microscope image of the FET are shown in Figure 8a. There is a narrow edge (green edge and circled out) around the FET device, which will be discussed in detail later. Additionally, the cracks at the surface were generated by the device fabrication process. The thin film may have folded due to the stress, thus creating cracks. The thickness of the FeS_2 thin film is approximately 35 nm, as measured by a profilometer, which is 3.5 times that of the iron thin film precursor deposited by e-beam evaporation. The expansion factor is consistent with other reported results.[14,32] The transfer curve (I_{ds} vs. V_g) and output curve (I_{ds} vs. V_{ds}) are shown in Figures 8b and 8c, respectively. The device edge is also clearly shown in the insert image of Figure 8b. An I_{on}/I_{off} ratio of 3.94×10^4 was obtained, which is larger than for any other FeS_2 FET devices reported. Two steps are needed to increase the I_{ds} in the transfer curve. The first step, which has an I_{on}/I_{off} ratio of approximately 10^4, is caused by the edge effect caused by the thin slice mentioned above. Although increasing the V_g will overcome the edge effect, the device will fully turn on at approximately V_g = -25 V. Although the change is small, the I_{ds}-V_{ds} in Figure 8c shows that the active channel of the device can be modulated by the gate

RSC Advances Accepted Manuscript

This journal is © The Royal Society of Chemistry 20xx

voltage. No saturation is observed in the output curve of the device, which indicates that further investigation is needed to increase the resistivity and reduce the carrier concentration of the FeS_2 thin film. The details of the electrical performance of the FeS_2 FET device are listed in Table 2. The device mobility requires attention because it is lower than the Hall mobility of the FeS_2 thin film that was measured using the Resistivity/Hall system. This may be due to the thick gate dielectric that lowers the control ability of the gate voltage over the active channel. High-k dielectric materials, including Al_2O_3 and ZrO_2, may increase the device mobility and enhance its performance.[45]
To test the electrical contact used in the device, Figure 8d shows the transmission line method (TLM) test of the FeS_2 devices. The linear slope shows the ohmic contact for the FeS_2 thin film. According to the slope, the device has a sheet resistance of approximately 3467 Ω/sq, and the sheet resistance observed via the TLM is smaller than recorded using the Resistivity/Hall Measurement System, which may be due to the low contact resistance of the metal contact. Instead of pristine silver paste, a stack layer of Ti/Ni/Au was deposited by E-beam evaporation with the thickness 10nm/90nm/20nm. Here, the thin Ti layer was used as the glue layer to improve the contact of the metal electrode with the FeS_2 thin film. . The layer of gold was used to reduce the contact resistance between the probes and the metal pads of devices during the measurement. Thus, the metal exhibited a low series resistance of approximately 1827 Ω, which is shown at the plot intercept in Figure 8d.[46]

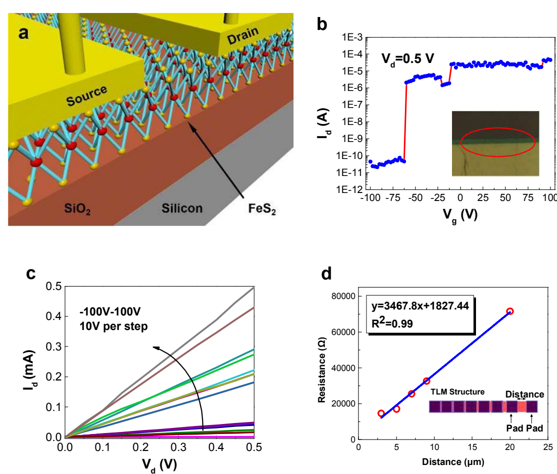

Figure 8. (a) Schematic of the FeS_2 FET device, (b) the I_{ds}-V_g with the image of channel edge, (c) the I_d-V_d curve and (d) the Resistance vs Distance curve with the layout of the pads and TLM Structure.

Table 2. Parameters of the FeS_2 FET device

Parameter	Value	Unit	Parameter	Value	Unit
W/L	40/2	µm	On-Off Ratio	3.94E+4	
Gate dielectric layer thickness	300	nm	Vth	-25	V
Cox	1.15E-04	$F \cdot m^{-2}$	Device Mobility	0.223	$cm^2 V^{-1} s^{-1}$
On-State Resistance	4.38E5	Ω	gm	0.256	µS
Off Current	2.97E-9	A	ρ	0.96	Ω·cm
On Current	1.17E-4	A	Carrier Concentration	2.94E19	cm^{-3}

Although the I_{on}/I_{off} ratio is much higher than previous reported FeS_2 transistor, it is still low for further application in electronics area. In order to reveal the problem that cause the low I_{on}/I_{off} ratio, we studied the electrical transport mechanisms of the FeS_2 thin film using a temperature-dependent four probe electrical measurement. Figure 9a shows the I_{ds}-V_{ds} curves at different temperatures. The resistance of the active channel increased as the temperature decreased. The conductivity was calculated using the parameters of the FeS_2 device. Figure 9b is plotted as ln(σ) versus $T^{1/4}$, and we obtained a linear relationship for low temperature. This finding indicates that the conductivity follows the Mott VRH mechanism:[47]

$$\sigma = \sigma_0 \exp[-(T_0/T)]^{1/4},$$

where σ_0 is the prefactor and T_0 is the Mott VRH temperature.[48] This mechanism indicates that the electron is hopping among localized states in the disordered system.[49,50] In the FeS_2 thin film, the disorder is attributed to the random distribution of defects and impurities that results in the localization of charge carriers.[48,51] As we discussed in the XPS section, the FeS_2 thin film is a defect-rich system. Combined with the FET transport behaviour, these results suggest that the electrical transport is primarily influenced by localized defects in the crystalline FeS_2 thin film.

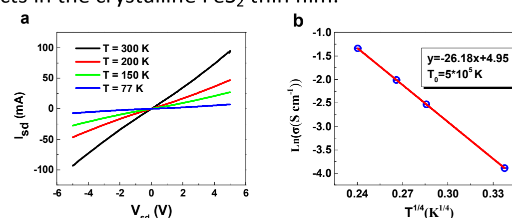

Figure 9. Temperature dependence of the FeS_2 samples

Conclusion

We demonstrated a successful method for synthesizing an ultrathin FeS_2 thin film via thermal sulfidation of an iron thin film. The phase of the FeS_2 thin film was confirmed using TFXRD and Raman spectroscopy. Although a small amount of marcasite is present, the FeS_2 thin film obtained using 240 min

RSC Advances Accepted Manuscript

of sulfidation exhibits the best electrical properties, including resistivity, mobility and carrier concentration, for FET applications. Given the quality of the FeS_2 thin film, we fabricated a FET device with an I_{on}/I_{off} ratio of approximately $4*10^4$. Although the device is relatively difficult to control with the gate voltage, the potential for the use of FeS_2 in FET applications was demonstrated. The electron transport mechanism was also studied using temperature-dependent electrical transport measurements. The methodology used to generate the thin film and FET device provides a versatile platform to further improve the quality of FeS_2 thin films as promising candidates in FET materials.

We found that our polycrystalline film has many surface defects and grain boundaries, which sharply reduce the material's quality and device performance. These are also an issue for FeS_2 photovoltaic solar cells. A high density surface state will cause high recombination, which limits the conversion efficiency. The low mobility of the FET device is the main challenge limiting the utility of FeS_2. To enhance the mobility of the device, we believe that a high k-dielectric gate layer and an effective passivation layer are the solution.[34,45] High k-dielectric materials reduce the gate layer thickness and increase the control ability of the gate voltage, whereas the passivation layer can reduce the surface defect states. Both methods could further enhance the channel modulation capability of FeS_2 devices.

Acknowledgements

This work is supported by startup funding of Sun Yat-sen University−Carnegie Mellon University Joint Institute of Engineering (Funding No. 47000-18811300) and startup funding of Sun Yat-sen University−Carnegie Mellon University Shunde International Joint Research Institute (Funding No. 20140303).

The authors would also like to thank Mr. Guijun Li, Mr. Meng Zhang and staff in PSKL. The authors also would like to thank Prof. Kei May Lau, Mr. Wilson Tang, and staff in Photonic Technology Center (PTC), Nanoelectronic Fabrication Facility (NFF), and Material Characterization & Preparation Facility (MCPF).

Reference

1 F. Alharbi, J. D. Bass, A. Salhi, A. Alyamani, H. C. Kim and R. D. Miller, *Renew. Energy*, 2011, **36**, 2753–2758.
2 J. Oertel, K. Ellmer, W. Bohne, J. Ro and H. Tributsch, *J. Cryst. Growth*, 1999, **199**, 1205–1210.
3 G. Willeke, R. Dasbach, B. Sailer and E. Bucher, *Thin Solid Films*, 1992, **213**, 271–276.
4 L. Meng and M. S. Liu, *Mater. Sci. Eng. B Solid-State Mater. Adv. Technol.*, 1999, **60**, 168–172.
5 W. Dong and C. Zhu, *J. Mater. Chem.*, 2002, **12**, 1676–1683.
6 D. G. Moon, A. Cho, J. H. Park, S. Ahn, H. Kwon, Y. S. Cho and S. Ahn, *J. Mater. Chem. A*, 2014, **2**, 17779–17786.
7 X. Shi, A. Tian, X. Xue, H. Yang and Q. Xu, *Mater. Lett.*, 2015, **141**, 104–106.
8 A. Ennaoui and H. Tributsch, *Sol. Energy Mater.*, 1986, **14**, 461–474.
9 M. Cabán-Acevedo, D. Liang, K. S. Chew, J. P. Degrave, N. S. Kaiser and S. Jin, *ACS Nano*, 2013, **7**, 1731–1739.
10 Y. Bi, Y. Yuan, C. L. Exstrom, S. a. Darveau and J. Huang, *Nano Lett.*, 2011, **11**, 4953–4957.
11 A. Ennaoui, S. Fiechter, C. Pettenkofer, N. Alonso-Vante, K. Büker, M. Bronold, C. Höpfner and H. Tributsch, *Sol. Energy Mater. Sol. Cells*, 1993, **29**, 289–370.
12 K. J. Andersson, H. Ogasawara, D. Nordlund, G. E. Brown and A. Nilsson, *J. Phys. Chem. C*, 2014, **118**, 21896–21903.
13 M. Cabán-Acevedo, N. S. Kaiser, C. R. English, D. Liang, B. J. Thompson, H.-E. Chen, K. J. Czech, J. C. Wright, R. J. Hamers and S. Jin, *J. Am. Chem. Soc.*, 2014, **136**, 17163–79.
14 X. Zhang, M. Manno, A. Baruth, M. Johnson, E. S. Aydil and C. Leighton, *ACS Nano*, 2013, **7**, 2781–2789.
15 C.-H. Liu, C.-H. Chen, S.-Y. Chen, Y.-T. Yen, W.-C. Kuo, Y.-K. Liao, J.-Y. Juang, H.-C. Kuo, C.-H. Lai, L.-J. Chen and Y.-L. Chueh, *Nano Lett.*, 2011, **11**, 4443–8.
16 Y.-C. Wang, H.-Y. Cheng, Y.-T. Yen, T.-T. Wu, C.-H. Hsu, H.-W. Tsai, C.-H. Shen, J.-M. Shieh and Y.-L. Chueh, *ACS Nano*, 2015, **9**, 3907–16.
17 D.-Y. Wang, M. Gong, H.-L. Chou, C.-J. Pan, H.-A. Chen, Y. Wu, M.-C. Lin, M. Guan, J. Yang, C.-W. Chen, Y.-L. Wang, B.-J. Hwang, C.-C. Chen and H. Dai, *J. Am. Chem. Soc.*, 2015, **137**, 1587–92.
18 N. Berry, M. Cheng, C. L. Perkins, M. Limpinsel, J. C. Hemminger and M. Law, *Adv. Energy Mater.*, 2012, **2**, 1124–1135.
19 J. Hu, Y. Zhang, M. Law and R. Wu, *Phys. Rev. B - Condens. Matter Mater. Phys.*, 2012, **85**, 1–10.
20 R. Morrish, R. Silverstein and C. a Wolden, *J. Am. Chem. Soc.*, 2012, **134**, 17854–7.
21 M. Bronold, S. Kubala, C. Pettenkofer and W. Jaegermann, *Thin Solid Films*, 1997, **304**, 178–182.
22 H. Liu and D. Chi, *J. Vac. Sci. Technol. A Vacuum, Surfaces, Film.*, 2012, **30**, 04D102.
23 L. Huang, F. Wang, Z. Luan and L. Meng, *Mater. Lett.*, 2010, **64**, 2612–2615.
24 Y. Z. Dong, Y. F. Zheng, H. Duan, Y. F. Sun and Y. H. Chen, *Mater. Lett.*, 2005, **59**, 2398–2402.
25 S. Shukla, N. H. Loc, P. P. Boix, T. M. Koh and R. R. Prabhakar, *ACS Nano*, 2014, **8**, 10597–10605.
26 L. Li, M. Cabán-Acevedo, S. N. Girard and S. Jin, *Nanoscale*, 2014, **6**, 2112–8.
27 M. Gong, A. Kirkeminde, Y. Xie, R. Lu, J. Liu, J. Z. Wu and S. Ren, *Adv. Opt. Mater.*, 2013, **1**, 78–83.
28 G. Srivastava, C. K. Das, A. Das, S. K. Singh, M. Roy, H. Kim, N. Sethy, A. Kumar, R. K. Sharma, S. K. Singh, D. Philip and M. Das, *RSC Adv.*, 2014, **4**, 58495–58504.
29 F. A. Rasmussen and K. S. Thygesen, *J. Phys. Chem. C*, 2015, 150430115624006.
30 M. Cabán-Acevedo, M. S. Faber, Y. Tan, R. J. Hamers and S. Jin, *Nano Lett.*, 2012, **12**, 1977–1982.
31 M. Limpinsel, N. Farhi, N. Berry, J. Lindemuth, C. L. Perkins, Q. Lin and M. Law, *Energy Environ. Sci.*, 2014, **7**, 1974.
32 Y. H. Liu, L. Meng and L. Zhang, *Thin Solid Films*, 2005, **479**, 83–88.
33 K. Sun, Z. Su, J. Yang, Z. Han, F. Liu, Y. Lai, J. Li and Y. Liu, *Thin Solid Films*, 2013, **542**, 123–128.

RSC Advances Accepted Manuscript

This journal is © The Royal Society of Chemistry 20xx

34 D. Liang, M. Cabán-Acevedo, N. S. Kaiser and S. Jin, *Nano Lett.*, 2014, **14**, 6754–60.
35 F. Withers, O. Del Pozo-Zamudio, a. Mishchenko, a. P. Rooney, a. Gholinia, K. Watanabe, T. Taniguchi, S. J. Haigh, a. K. Geim, a. I. Tartakovskii and K. S. Novoselov, *Nat. Mater.*, 2015, **14**, 301–306.
36 S. Fiechter, M. Birkholz, A. Hartmann, P. Dulski, M. Giersig, H. Tributsch and R. J. D. Tilley, *J. Mater. Res.*, 1992, **7**, 1829–1838.
37 C. de las Heras, J. L. M. de Vidales, I. J. Ferrer and C. Sánchez, *J. Mater. Res.*, 2011, **11**, 211–220.
38 X. Qiu, M. Liu, T. Hayashi, M. Miyauchi and K. Hashimoto, *Chem. Commun. (Camb).*, 2013, **49**, 1232–4.
39 H. Vogt, T. Chattopadhyay and H. J. Stolz, *J. Phys. Chem. Solids*, 1983, **44**, 869–873.
40 A. K. Kleppe and A. P. Jephcoat, *Mineral. Mag.*, 2004, **68**, 433–441.
41 M. Bronold, Y. Tomm and W. Jaegermann, *Surf. Sci.*, 1994, **314**, L931–L936.
42 F. W. Herbert, A. Krishnamoorthy, W. Ma, K. J. Van Vliet and B. Yildiz, *Electrochim. Acta*, 2014, **127**, 416–426.
43 J. Xu, H. Xue, X. Yang, H. Wei, W. Li, Z. Li, W. Zhang and C.-S. Lee, *Small*, 2014, 1–6.
44 J. P. Degrave, D. Liang and S. Jin, *Nano Lett.*, 2013, **13**, 2704–2709.
45 B. Radisavljevic, A. Radenovic, J. Brivio, V. Giacometti and A. Kis, *Nat. Nanotechnol.*, 2011, **6**, 147–50.
46 R. J. Soukup, P. Prabukanthan, N. J. Ianno, A. Sarkar, C. a. Kamler and D. G. Sekora, *J. Vac. Sci. Technol. A Vacuum, Surfaces, Film.*, 2011, **29**, 011001.
47 C. Lu, Q. Fu, S. Huang and J. Liu, *Nano Lett.*, 2004, **4**, 623–627.
48 N. F. Mott, *Mott-Insulator Transition*, Taylor-Francis: London, London, 1990.
49 D. Lichtenberger, K. Ellmer, R. Schieck, S. Fiechter and H. Tributsch, *Thin Solid Films*, 1994, **246**, 6–12.
50 K. Ellmer, D. Lichtenberger, A. Ennaoui, C. Hopfner, S. Fiechter and H. Tributsch, in *Conference Record of the Twenty Third IEEE Photovoltaic Specialists Conference - 1993 (Cat. No.93CH3283-9)*, IEEE, 1993, pp. 535–538.
51 A. L. Shklovskii, B.I., Efros, *Electronic Properties of Doped Semiconductors*, Springer-Verlag, Berlin.

RSC Advances Accepted Manuscript